Impact of Tropical SST on Stratospheric Planetary Waves in the Southern Hemisphere

PU LIN, QIANG FU,* AND DENNIS L. HARTMANN

Department of Atmospheric Sciences, University of Washington, Seattle, Washington

(Manuscript received 9 July 2011, in final form 21 January 2012)

ABSTRACT

The impact of tropical sea surface temperature (SST) on stratospheric planetary waves in the Southern Hemisphere (SH) is investigated in austral spring using observed SST and reanalysis data for the past three decades. Maximum covariance analysis indicates that the tropical SST and the SH stratospheric planetary wave activity are primarily coupled through two modes. The leading two modes show the La Niña–like and the central-Pacific El Niño–like SST anomalies in their positive polarities, respectively, which each are related to enhanced stratospheric planetary wave activity. These two modes also introduce phase shifts to the stratospheric stationary planetary waves: a westward shift is seen for La Niña and an eastward shift for warm SST anomalies is seen in the central Pacific. The Eliassen–Palm fluxes associated with the two modes indicate that the anomalous stratospheric wave activity originates in the troposphere and propagates upward over the mid–high latitudes, so that the linkages between tropical SST and extratropical tropospheric circulation appear to play a key role. Furthermore, the observed circulation anomaly patterns for the two modes change rapidly from spring to summer, consistent with a sharp seasonal transition in the SH basic state. Similar SST and circulation anomaly patterns associated with the two modes are simulated in chemistry–climate models.

1. Introduction

Planetary wave activity accounts for a large portion of the spatial and temporal variability of the stratosphere. Its interaction with the zonal-mean flow affects the strength and the duration of the polar vortex (e.g., Mechoso et al. 1985; Polvani and Plumb 1992). Planetary wave breaking is the major driver of the equator-to-pole hemispheric Brewer–Dobson circulation (BDC) in the stratosphere (e.g., Rosenlof and Holton 1993; Holton et al. 1995). Stratospheric planetary waves also play an important role in shaping the ozone hole (e.g., Austin and Butchart 1992; Solomon 1999; Fusco and Salby 1999) and its recovery (e.g., Li et al. 2009; Oman et al. 2010) by affecting the polar vortex and BDC.

Stratospheric planetary waves are mainly generated in the troposphere and propagate upward (e.g., Mechoso et al. 1985; Holton et al. 1995). Tropical sea surface temperature (SST) is an important thermal forcing for the stationary waves in the extratropics. Previous model analyses (Kasahara and da Silva Dias 1986; Quintanar and Mechoso 1995; Inatsu and Hoskins 2004) suggested that tropical SST is the dominant forcing for the SH stationary planetary waves. Grassi et al. (2008) linked the anomalous wave activity in the SH and the consequent stratosphere sudden warming in 2002 to tropical SST preconditions.

Recent atmospheric general circulation model (AGCM) and chemistry–climate model (CCM) simulations also emphasize the role that tropical SST plays in modifying stratospheric circulation. Li et al. (2010) found in an AGCM that tropical Indian Ocean warming can force Rossby wave trains in the extratropics and induce opposite annular responses in the Northern and Southern Hemispheres. Using an AGCM, Hu and Fu (2009) attributed the enhanced stratospheric wave activity and thus the stronger BDC in the SH since 1979 partly to tropical SST warming. Recent CCM simulations also suggested that the warmer tropical SST under climate change would lead to a stronger wave-driven tropical upwelling in the lower stratosphere, either directly by enhancing the tropical waves (Deckert and Dameris 2008) or indirectly through its modification of the

* Additional affiliation: College of Atmospheric Sciences, Lanzhou University, Lanzhou, China.

Corresponding author address: Pu Lin, Department of Atmospheric Sciences, University of Washington, Box 351640, Seattle, WA 98105. E-mail: plin@atmos.washington.edu

DOI: 10.1175/JCLI-D-11-00378.1

subtropical jets (e.g., Eichelberger and Hartmann 2005; Olsen et al. 2007; Oman et al. 2009; Shepherd and McLandress 2011).

Since the leading mode of tropical SST variability on the interannual time scales is the El Niño–Southern Oscillation (ENSO) (e.g., Kawamura 1994), many efforts have been made to detect and understand the linkage between ENSO and the extratropical stratospheric circulation (e.g., Camp and Tung 2007; Garfinkel and Hartmann 2007; Free and Seidel 2009; Sassi et al. 2004). These studies focused on NH winter showing stronger stratospheric planetary waves during El Niño events, which further lead to weaker polar vortex, stronger BDC, tropical stratospheric cooling, and polar stratospheric warming. But much less attention has been given to the SH. Recent literature recognized a new type of El Niño referred to as ''dateline El Niño'' (Larkin and Harrison 2005), ''El Niño Modoki'' (Ashok et al. 2007), ''central-Pacific El Niño'' (Kao and Yu 2009), or ''warm pool El Niño'' (Kug et al. 2009) (hereafter central-Pacific El Niño). Ding et al. (2011) linked the recent West Antarctica warming with central-Pacific El Niño events. Hurwitz et al. (2011) found stronger SH planetary waves during central-Pacific El Niño events, but no clear signal in the SH stratosphere for conventional El Niño events.

In this study, we investigate the linkage between the tropical SST and the SH stratospheric planetary wave activity during austral spring by using maximum covariance analysis (MCA). Robust circulation patterns are found to be associated with tropical SST anomalies. We find that the SST–stratosphere linkage in SH spring is different from that in NH winter shown in earlier studies (e.g., Camp and Tung 2007; Garfinkel and Hartmann 2007; Free and Seidel 2009; Sassi et al. 2004). Herein the SST–stratosphere linkage is examined in 3D space and its monthly dependence is investigated. These analyses enable us to identify signals that were masked in Hurwitz et al. (2011). In the following, section 2 describes the datasets and analysis methods used in this study. Section 3 presents the results. Section 4 discusses the plausible mechanisms and implications of the results. A summary and conclusions are given in section 5.

2. Data and methodology

In this study, we use the observed SST dataset of the monthly-mean Extended Reconstruction Sea Surface Temperature, version 3b (ERSST.v3b; Smith et al. 2008). SST data from the Met Office Hadley Centre Sea Ice and Sea Surface Temperature, version 1 (HadISST1; Rayner et al. 2003), has also been analyzed and yields almost identical results. For atmospheric variables, we use monthly-mean geopotential height and wind from reanalysis data. We also calculate Eliassen–Palm (EP) flux from reanalysis daily data. Five different reanalysis datasets are examined. They are the 40-yr European Centre for Medium-Range Weather Forecasts (ECMWF) Reanalysis (ERA-40; Uppala et al. 2005), the National Centers for Environmental Prediction–National Center for Atmospheric Research reanalysis (NCEP–NCAR; Kalnay et al. 1996), NCEP–Department of Energy Reanalysis 2 (Kanamitsu et al. 2002), the Japanese 25-year Reanalysis (JRA-25; Onogi et al. 2007), and the Modern-Era Retrospective Analysis for Research and Applications (MERRA; Rienecker et al. 2011). Results from different reanalyses are similar to each other. Thus, unless otherwise specified, we present results based on JRA-25, since it extends higher into the stratosphere.

Among the five reanalysis datasets, only ERA-40 and NCEP–NCAR have data before 1979. Because the data since 1979 are more reliable due to the introduction of satellite observations, we focus on the period 1979–2009 but use the data from the earlier period as an independent check. All data were linearly detrended before the analysis. To avoid an artificial jump in the data due to the introduction of satellite data in 1979, we detrended the data separately for the periods before and after 1979.

We compare the CCM simulations with the observational results. We use 14 CCM simulations participating in the Chemistry–Climate Model Validation activity, phase 2 (CCMVal-2; Eyring et al. 2005; SPARC CCMVal 2010). The 14 CCMs are the Atmospheric Model with Transport and Chemistry, version 3 (AMTRAC3), the Community Atmosphere Model, version 3.5 (CAM3.5), the Center for Climate System Research–National Institute for Environmental Studies (CCSRNIES) model, the ECHAM/Modular Earth Submodel System Atmospheric Chemistry (EMAC) model, the Goddard Earth Observing System Chemistry Climate Model (GEOS CCM), the Laboratoire de Météorologie Dynamique Model with Zoom Capability–Reprobus (LMDZrepro), the Meteorological Research Institute (MRI) model, the National Institute of Water and Atmospheric Research Solar Climate Ozone Links (NIWA-SOCOL) model, SOCOL, the University of L'Aquila (ULAQ) model, the Unified Model Single Layer Isentropic Model of Chemistry and Transport (UMSLIMCAT), the Unified Model/U.K. Chemistry Aerosol Community Model, Met Office version (UMUKCA-METO), Unified Model/U.K. Chemistry Aerosol Community Model, University of Cambridge version (UMUKMO-UCAM), and the Whole Atmosphere Community Climate Model (WACCM) (SPARC CCMVal 2010). These models all have relatively good representations of stratospheric dynamical, radiative, and chemical processes but vary in their detailed representation of the physical processes. We

used the simulations under the B1 reference (REF-B1) scenario, which is a transient scenario intended to reproduce climate changes over the past few decades. The models are forced with the observed greenhouse gases and ozone-depleting substances, and with observed SST and sea ice concentrations from HadISST1. More details of these models and simulations can be found in SPARC CCMVal (2010) and the references therein.

We have carried out the analysis from late winter to early summer with a focus on September. This is because stratospheric planetary wave activity is the strongest during late winter to spring in the SH (Randel 1988). September is the month when the observed circulation change in the SH stratosphere is the strongest in the last three decades (Lin et al. 2009; Fu et al. 2010). It is also the month when the ozone hole starts to develop and interacts actively with stratospheric dynamics and radiation, and thus causes large circulation changes (Thompson and Solomon 2002).

The analysis method used is MCA (Bretherton et al. 1992; Wallace et al. 1992). MCA seeks out pairs of spatial patterns and associated time series that efficiently explain the covariance between two fields. The correlation coefficient between these time series indicates the strength of the coupling between the two patterns in the two fields. Heterogeneous regression maps of the patterns are produced by regressing the time series of the pattern amplitude of one field with the gridded data of the other field.

To examine the impact of the tropical SST on the SH stratospheric planetary wave activity, MCA is performed on SST over 20°N–20°S and geopotential height at 50 hPa (Z50) over 2.5°–80°S. Z50 is chosen as the indicator of the stratospheric circulation. The resulting patterns are insensitive to the choice of the stratospheric geopotential height level. Heterogeneous maps are shown to represent the spatial patterns associated with the covariance. We then made use of the SST time series associated with the leading modes, and regressed geopotential height and other variables upon them to identify the associated circulation anomalies at various pressure levels.

3. Results

a. MCA-generated patterns

As a first test, we calculated the normalized root-mean-squared covariance (RMSC) between the tropical SST and SH Z50. The RMSC should be greater than about 0.1 for well-correlated fields (Wallace et al. 1992). The RMSC between the two fields is 0.2, which justifies further exploration of the correlation.

Two pairs of patterns are able to explain ~83.0% of the squared covariance between tropical SST and SH Z50 on interannual time scales. These two pairs of patterns also closely resemble the first two leading modes in the interannual variability of SST and Z50, respectively, and together they explain 54.7% of the variance in SST and 52.5% of the variance in Z50.

Figure 1 shows the SST anomalies and geopotential height anomalies at five different levels associated with the first two modes identified by MCA. The time series of Z50 and SST for the two modes are also plotted. The time series are normalized to have a unit standard deviation, and so the magnitudes of the patterns are associated with one standard deviation in the time series of the mode. Climatological geopotential eddy fields are also plotted as contours for comparison. The squared covariance fraction explained by mode 1 and mode 2 is 57.9% and 25.1%, respectively. The Z50 and SST time series are correlated at 0.40 for mode 1 and at 0.60 for mode 2, both of which are significantly different from zero at the 95% confidence level after taking account of autocorrelation in these time series to reduce the effective degrees of freedom.

As shown in Fig. 1, mode 1 shows a La Niña–like SST pattern with an east–west seesaw pattern over the Pacific and mode 2 shows a central-Pacific El Niño–like SST pattern, with the largest variance over the central Pacific. Not surprisingly, the mode 1 time series shows a high correlation with the ENSO indicators, such as the cold tongue index (http://jisao.washington.edu/enso/) and the Niño-3.4 index (Trenberth 1997), and the mode 2 time series correlates well with the El Niño Modoki index (Ashok et al. 2007). Both modes show large-scale wave-like structure in the stratosphere, indicating a modification of the planetary waves there. The stratospheric anomalies of the two modes both show the strongest magnitudes along 60°S but have different phases. In mode 1, a La Niña–like SST pattern (cold anomalies over the east Pacific) is associated with negative stratospheric geopotential height anomalies over the eastern Pacific sector, and zonally elongated positive anomalies centered over the Eastern Hemisphere. In mode 2, warm SST anomalies over the central Pacific are associated with strong positive geopotential height anomalies over the Pacific sector and weak negative anomalies over the Indian and Atlantic sectors. The tropospheric geopotential height anomalies show more complex patterns along latitude than their stratospheric counterparts. The stratospheric anomaly patterns are roughly in phase with the tropospheric ones over the high latitudes, suggesting an equivalent barotropic connection between the tropospheric and the stratospheric anomalies. These patterns will be discussed in more detail in section 3c but before that, the robustness of these patterns is examined.

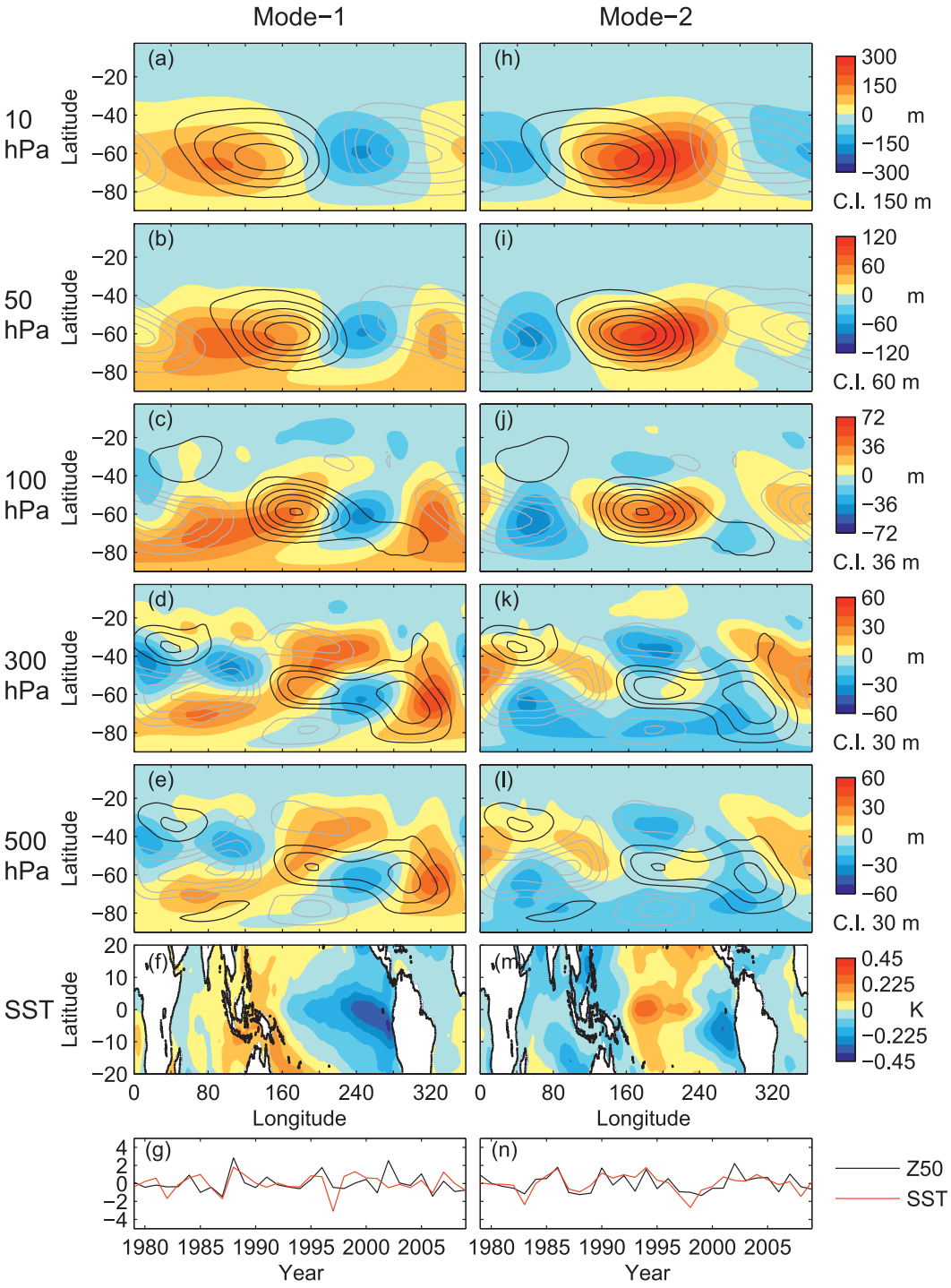

FIG. 1. Heterogeneous regression maps of mode 1 from MCA with geopotential height at (a) 10, (b) 50, (c) 100, (d) 300, and (e) 500 hPa, and (f) SST. (g) Corresponding time series for SST (red line) and Z50 (black line) of mode 1. (h)–(n) As in (a)–(g), but for mode 2. Climatological patterns of eddy geopotential height at each level are plotted as contours in (a)–(e) and (h)–(l). Positive contours are in black, and negative contours are in gray. Zero contours are omitted. Color scales and contour intervals are indicated on the right. Time series are normalized to have unit standard deviation. Unless otherwise specified, the presented results are based on JRA-25 along with the SST from the National Oceanic and Atmospheric Administration (NOAA) ERSST (Smith et al. 2008) for the period of 1979–2009.

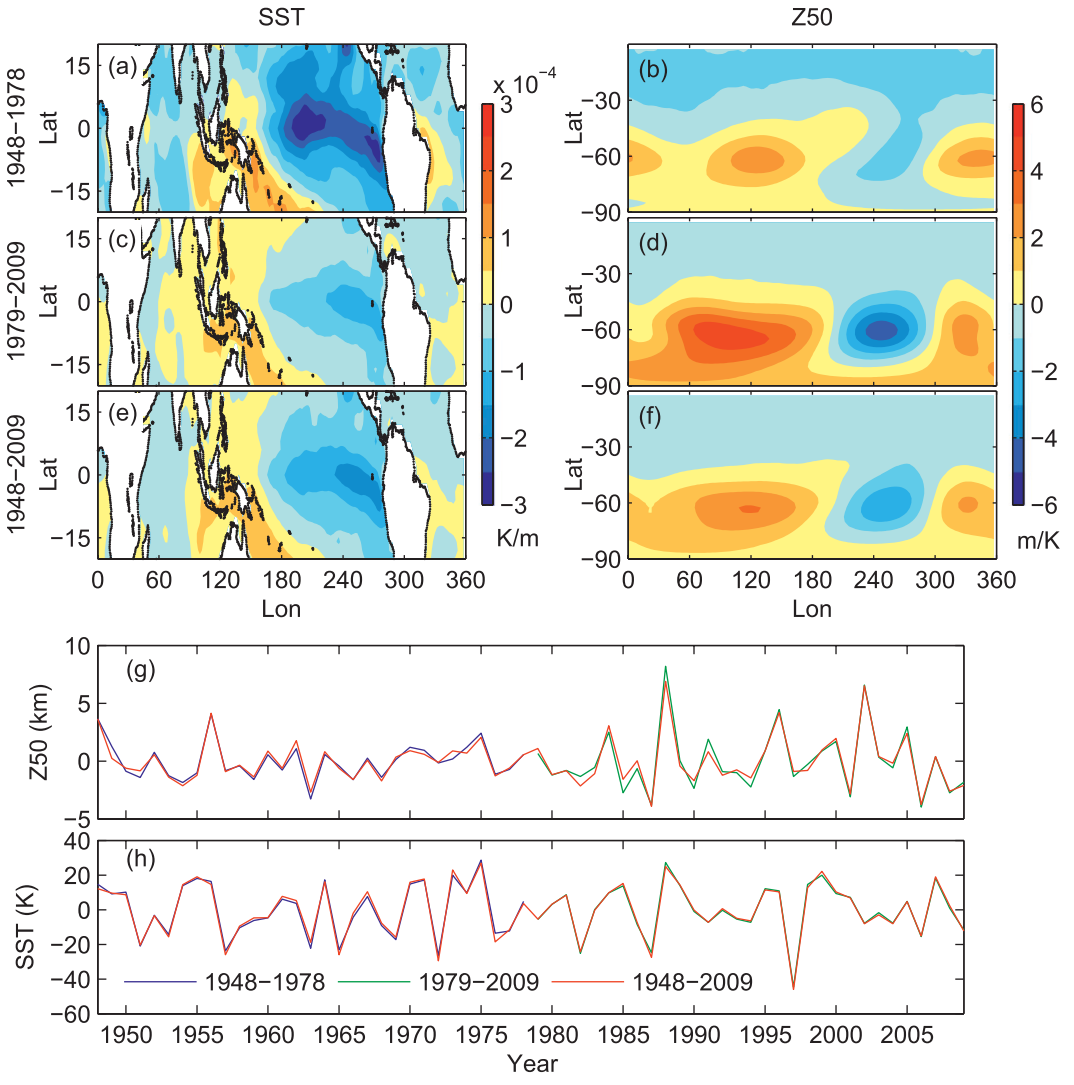

FIG. 2. Heterogeneous regression maps of mode 1 from MCA (a) with tropical SST 1948–78, (b) Z50 1948–78, (c) tropical SST 1979–2009, (d) Z50 1979–2009, (e) tropical SST 1948–2009, and (f) Z50 1948–2009, and corresponding time series for (g) Z50 and (h) SST. To compare the results from different periods, the time series are not normalized. NCEP–NCAR reanalysis data are used here for Z50.

b. Robustness of the patterns

As an independent check, we applied the same statistical technique to a different 31-yr period for 1948–78 and the whole 62 yr data for 1948–2009 from the NCEP–NCAR reanalysis. Figure 2 shows the first pair of SST and Z50 patterns and their time series for 1948–78, 1979–2009, and 1948–2009. The patterns from the earlier period (Figs. 2a,b), later period (Figs. 2c,d), and the whole period (Figs. 2e,f) are very similar from each other. The corresponding time series (Figs. 2g,h) from the two different periods are almost identical to those from the whole period. Figure 3 shows the second pair of SST and Z50 patterns and their time series for 1948–78, 1979–2009, and 1948–2009. While the mode 2 patterns from the earlier period (Figs. 3a,b) do not resemble those from the later period (Figs. 3c,d) very well, the patterns from the entire 62 yr of data (Figs. 3e,f) match well with those from the later period. It is worth noting that mode 2 from the earlier period explains a small fraction of the squared covariance, and it may not be significant as it is not distinguishable from mode 3 and above in terms of the fraction of explained covariance.

Similar analysis was done for the 45-yr ERA (1957–2001) (not shown). Despite its shorter record, ERA-40 also shows consistent SST and Z50 patterns before and after 1979 for mode 1. For mode 2, MCA for the post-1979 period shows similar results as for the whole period, but

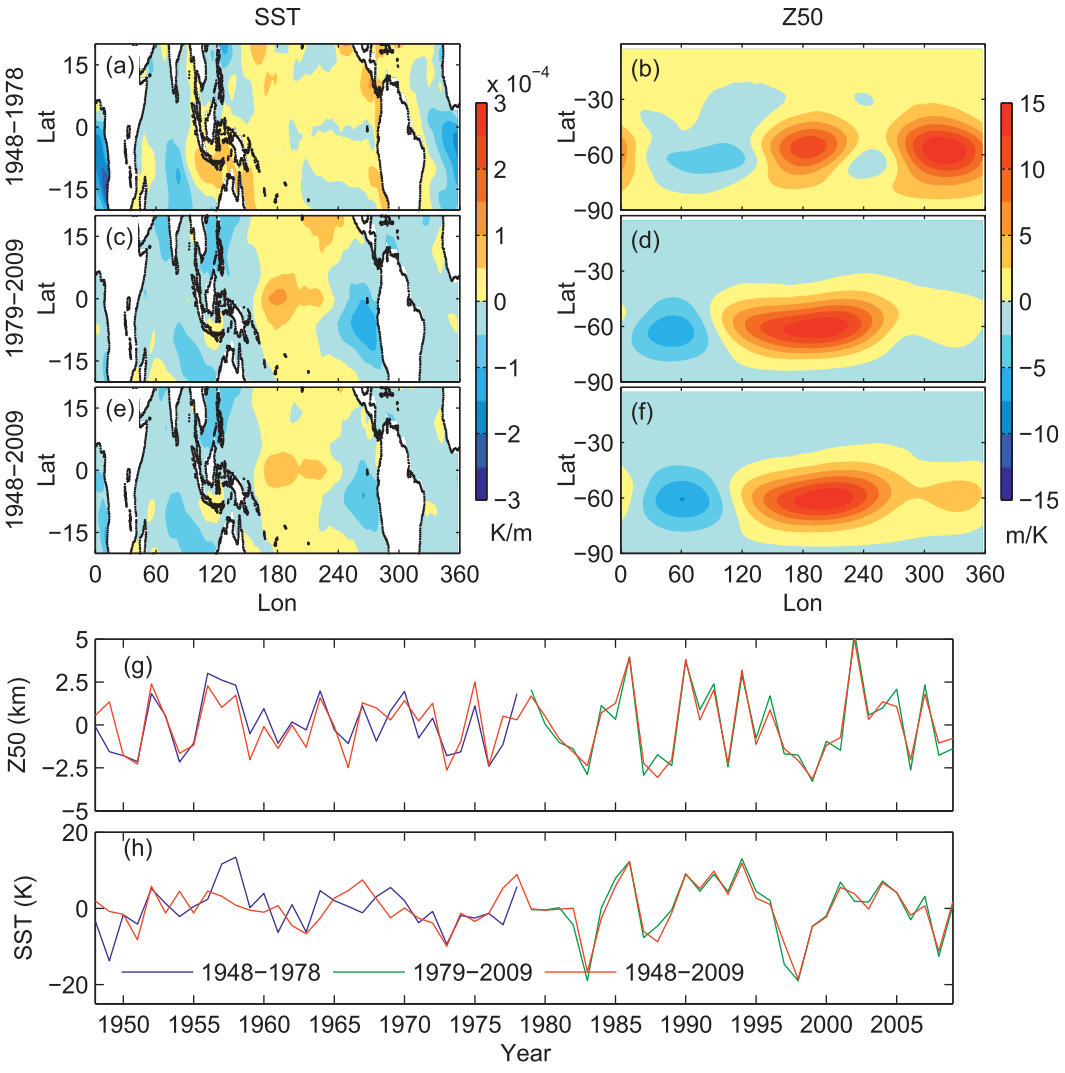

FIG. 3. As in Fig. 2, but for mode 2.

the patterns from the earlier period do not resemble those for the later period or the whole period.

The similarity of the patterns resulting from the two independent periods gives us confidence on the robustness of mode 1. In contrast, mode 2 shows less consistency between the pre-1979 and post-1979 periods, though part of the inconsistency could be related to the poor data quality in the SH prior to the advent of satellites.

The same statistical technique was applied to the CCM simulations. We used the multimodel mean geopotential height from 14 CCMs for 1960–2004 along with the prescribed SST fields in these models. MCA between Z50 from the models and SST yields two leading modes that can explain a large fraction of the squared covariance (72.1%, and 13.2%, respectively). The simulated mode 2 explains more covariance during the more recent years, which is consistent with observations. The correlation coefficient between the Z50 and SST time series is 0.57 for mode 1 and 0.55 for mode 2, both of which are significantly different from zero at the 95% confidence level.

Figure 4 shows the geopotential height and SST anomaly patterns associated with the two leading modes from the multimodel mean simulations, which show a similar structure as those from the observational data (Fig. 1). For the SST anomaly patterns, MCA using the model data identified an ENSO-like pattern as mode 1 and a central-Pacific ENSO-like pattern as mode 2, as in the observations. The associated geopotential height anomalies for the two modes from the models match with those from observations very well in the stratosphere, in terms of longitude of the ridges/troughs and the zonal and latitudinal structure. But the mode 2 pattern from the models is located more poleward than the observation. For the tropospheric anomalies, patterns from the models

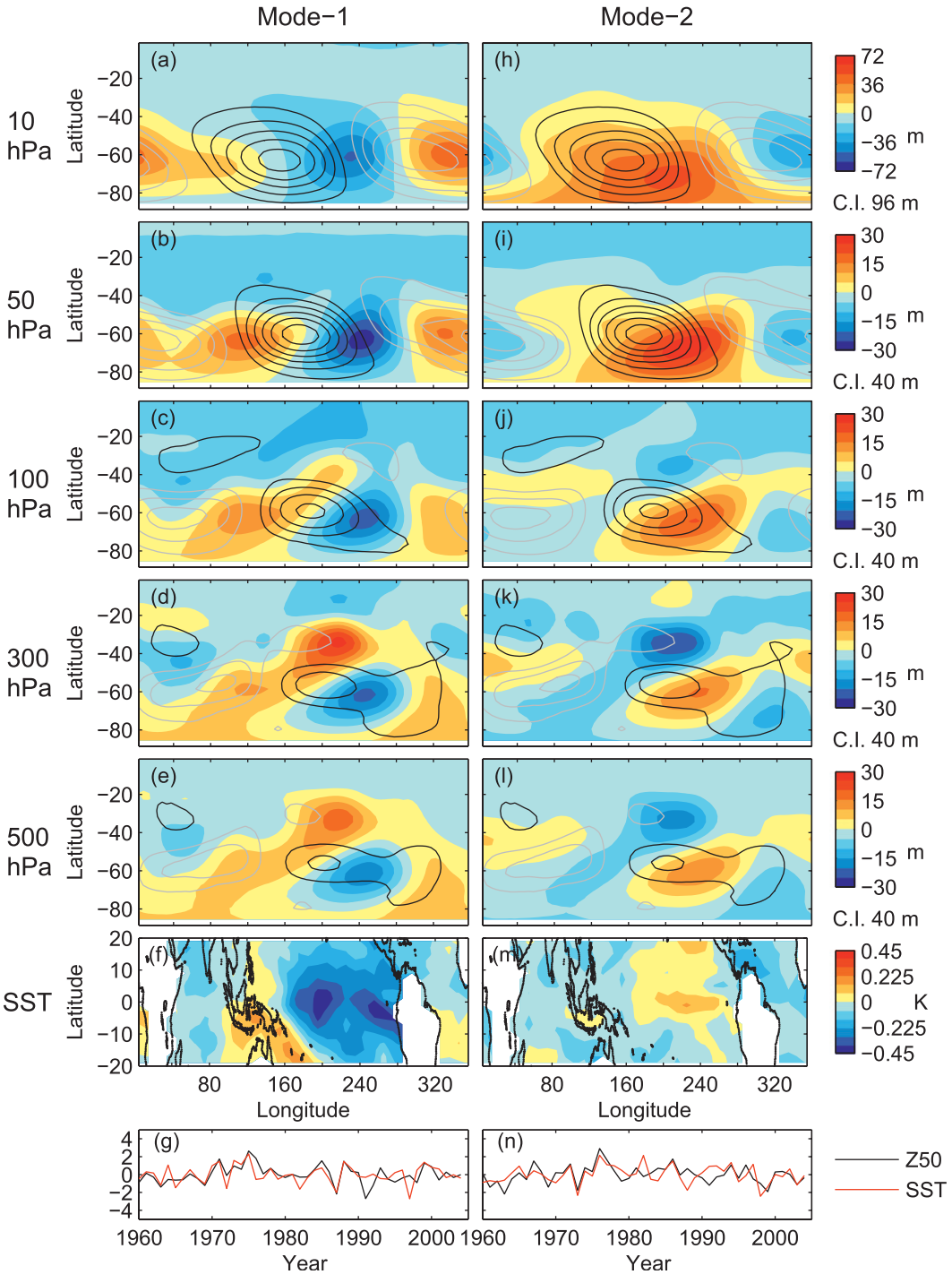

FIG. 4. As in Fig. 1, but the geopotential height is from the multimodel mean of 14 CCMs and the SST is from HadISST1 for 1960–2004.

show action centers at similar locations to those of observations. Modeled tropospheric anomaly patterns are stronger over the Pacific sector, but the observed patterns show comparable amplitude over all sectors. Note that these geopotential height anomaly patterns from the multimodel mean have much smaller amplitude than those from observations (~30% of the observations in the stratosphere and ~50% in the troposphere). Individual models can yield patterns with comparable amplitude to observations, but a large spread in the structure

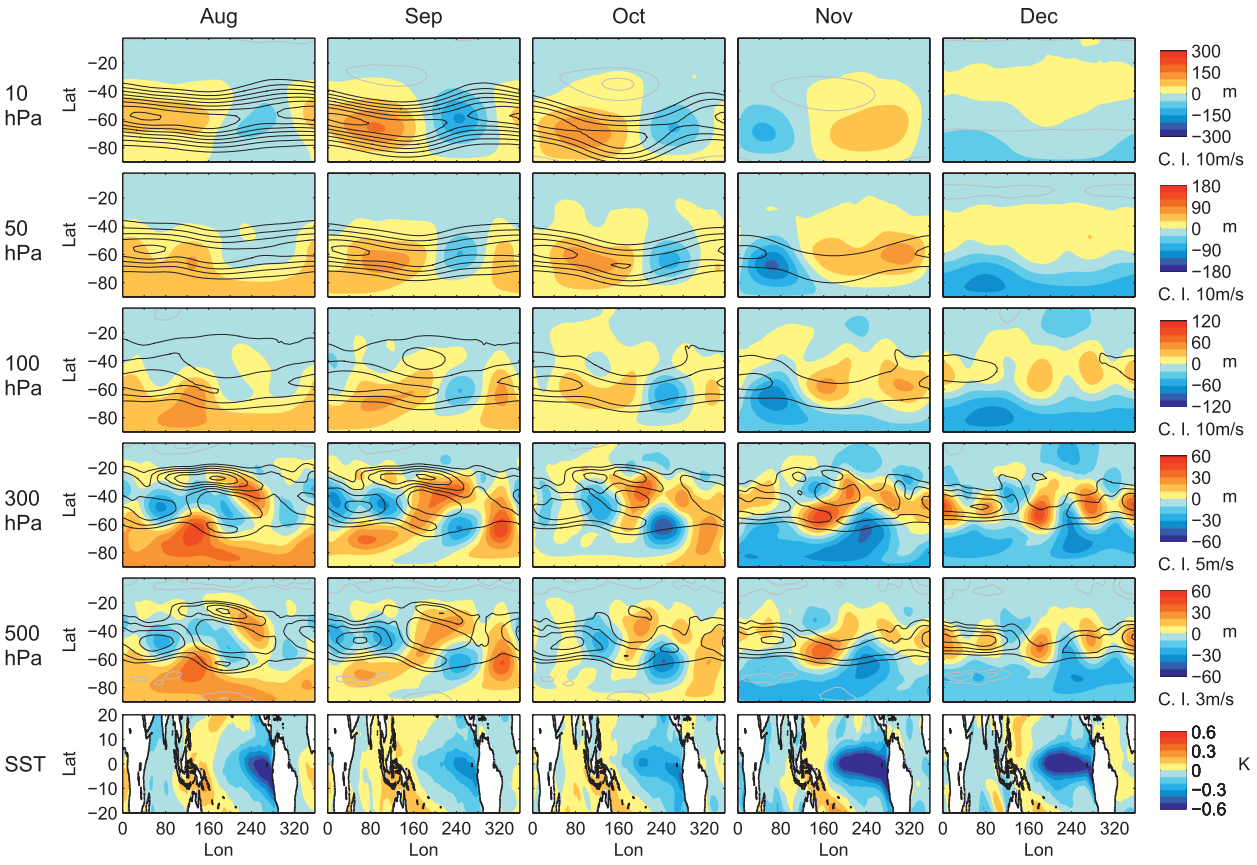

FIG. 5. Geopotential height anomalies at 10, 50, 100, 300, and 500 hPa, and the tropical SST anomalies associated with mode 1 in each month from August to December. Contours show the climatological zonal wind. Westerlies are plotted in black, and easterlies are plotted in gray. For clarity, weak westerlies (<20 m s^{-1} above 500 hPa and <15 m s^{-1} at 500 hPa) and zero wind are not plotted. Color scales and contour intervals are indicated on the right.

and the amplitude of the patterns is found among the models.

The SH stratosphere undergoes large changes from winter to summer, while tropical SST exhibits less seasonal change. Thus, it is interesting to examine this SST–stratosphere linkage in the context of the winter-to-summer transition. Figure 5 shows the mode 1 monthly geopotential height and SST anomaly patterns from August to December. The climatological zonal wind for each month is also plotted to indicate the basic state. In all these months, the leading mode of the SST–stratosphere coupling shows an ENSO-like SST pattern. The eastern Pacific action center of the SST patterns is located near the coast in August and extends westward in the later months. The associated geopotential height anomaly patterns in August and October are generally similar to those in September, but they show smaller amplitudes in the stratosphere. The stratospheric responses in November and December are weaker than earlier months and show a different phase compared to September. In the troposphere, a wave train–like structure extends from the exit of the subtropical jet poleward and eastward from September to November, but it is less discernible in August and December.

Figure 6 shows the monthly geopotential height and the SST anomaly patterns for mode 2. The SST patterns for this mode are similar from month to month, featuring a center of action over the equatorial central Pacific. The geopotential height anomalies associated with this mode show a ridge around 200°E in the stratosphere in August and September. This ridge moves eastward in October and November, and no clear ridge can be found in December. In the troposphere from August to November, a dipole structure is found over the Pacific sector with opposite anomalies centered at ~30°S, 180°E and ~60°S, 220°E. In December, the anomalies are much weaker than the earlier month, and the squared covariance fraction of mode 2 drops below 10%, suggesting that mode 2 may not contribute much variability in December.

We argue that different atmospheric responses to similar tropical SST patterns in different months are

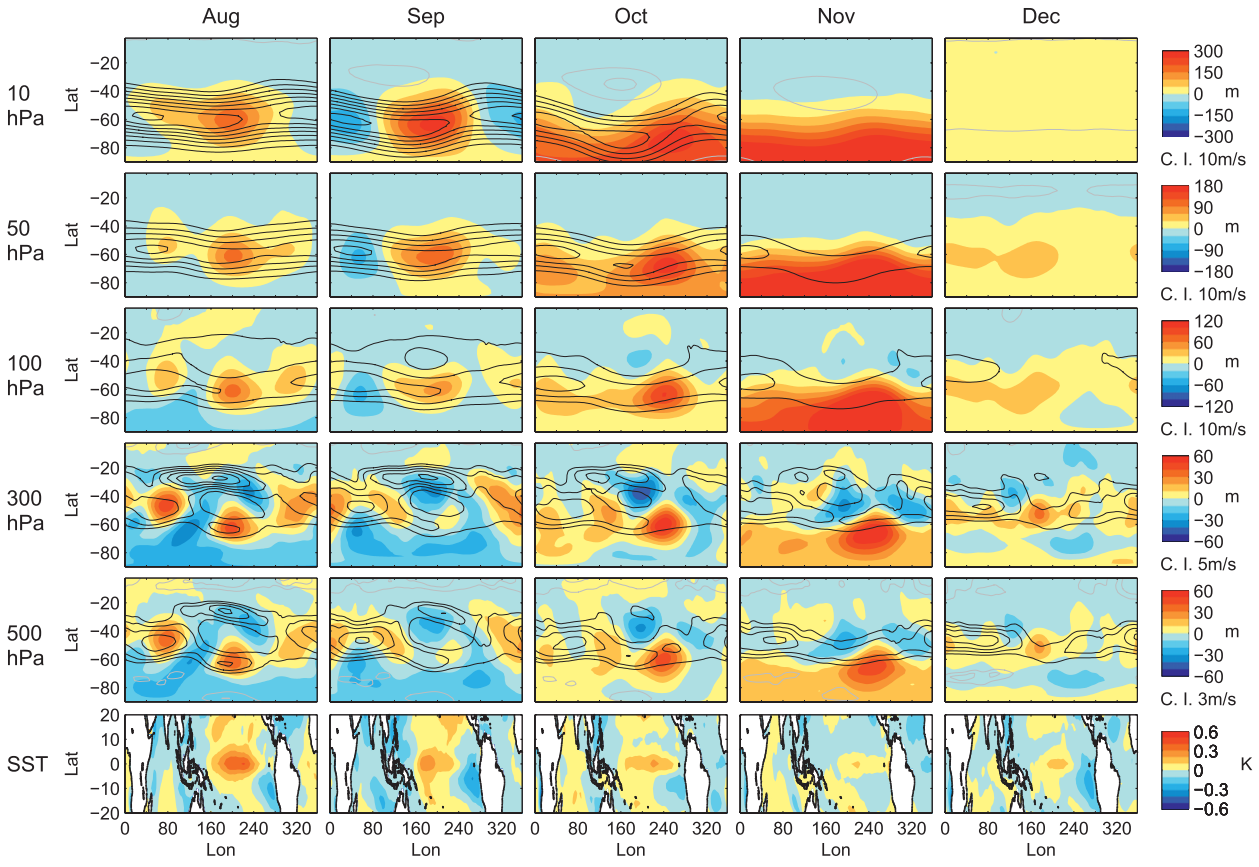

FIG. 6. As in Fig. 5, but for mode 2.

partly due to the difference in the basic state, especially the wind field. Zonal wind plays a crucial role in modifying the meridional and vertical propagation of waves (e.g., Karoly and Hoskins 1982). In August, the stratosphere shows a very strong polar vortex, and double jets can be seen in the Pacific sector in the troposphere. In November and December, the polar vortex breaks down and a weak westerly or easterly is found in the stratosphere. In the troposphere, the subtropical jet also becomes much weaker, and only one tropospheric jet appears in December. Given the dramatic difference in the zonal wind field from winter to summer (contours in Figs. 5, 6), it is not surprising that quite different geopotential height patterns are found in response to similar tropical SST patterns. From August to October, the background winds are more or less similar and thus similar circulation anomaly patterns are observed. Using the mean data in August–October yields a similar result to September. In contrast, the circulation anomaly patterns from the CCM simulations show stronger similarity from August to December (not shown) than those from observations. This may be linked to the delayed breakdown of the SH polar vortex in these CCM simulations (e.g., SPARC CCMVal 2010), and thus the simulated wind transition from August to December is less dramatic.

In summary, we find similar mode 1 patterns from an independent period of data, from adjacent months, and from CCM simulations. The combined evidence gives us confidence in the robustness of this mode. Patterns for mode 2 show less consistency among different analyses than mode 1, but they still give us reasonable confidence in its robustness. For the sake of completeness and to compare with earlier studies (Hurwitz et al. 2011), we present both modes and will discuss them in the following text.

c. *Interference with climatological waves*

In this section, we examine how these SST-related circulation patterns interfere with and modify the climatological planetary waves. Figure 1 shows that both the SST-related anomalies and the climatological eddy fields are dominated by low zonal wavenumbers. The typical amplitude for the mode 1 pattern is ~20% of that of the climatological eddy in the stratosphere and ~30% in the troposphere. The amplitude of mode 2 is ~35% in

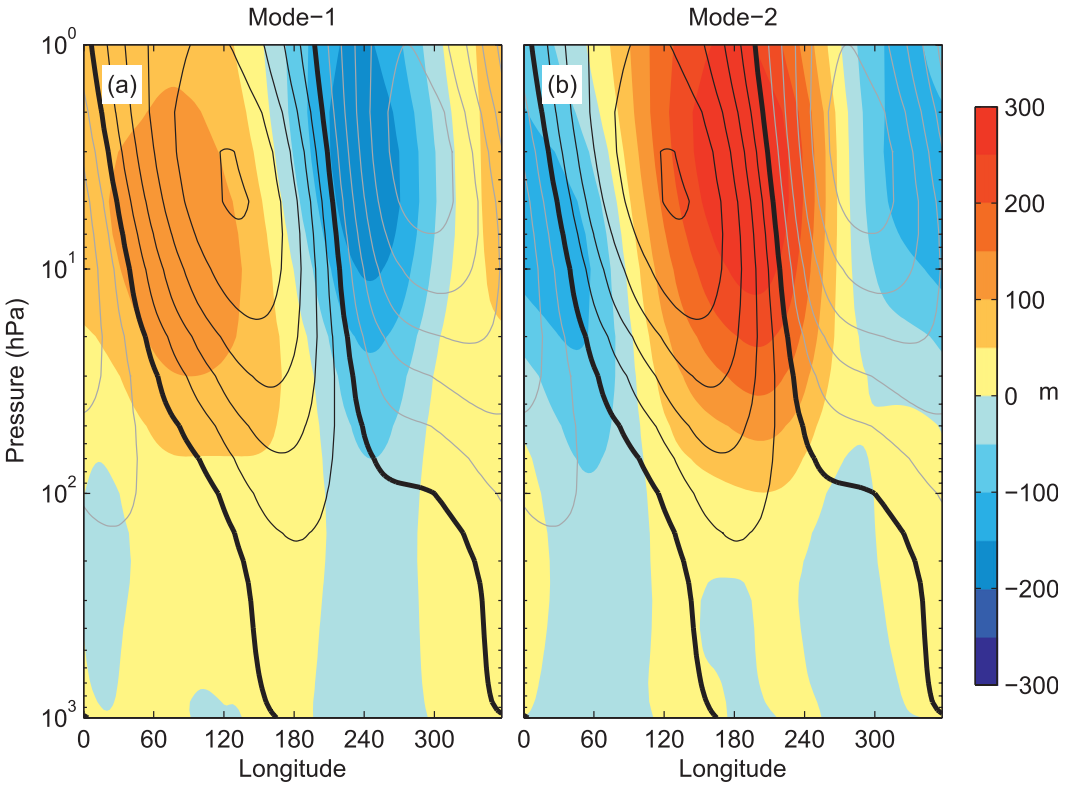

FIG. 7. Regression of geopotential height (color shading) upon the SST time series of (a) mode 1 and (b) mode 2 and the eddy geopotential height climatology (contours) at 60°S. Positive contours are plotted in thin black lines, negative contours are plotted in gray lines, and zero contours are plotted in thick black lines. Contour interval is 150 m.

the stratosphere and ~20% in the troposphere compared to the climatological eddy.

In the stratosphere, both the climatological eddy and SST-related anomalies show the largest amplitude along 60°S (Fig. 1). For mode 1 in its positive polarity (i.e., associated with the La Niña–like SST), the stratospheric geopotential height anomalies show ridges and troughs to the west of those in the climatology (Figs. 1a–c), indicating a westward shift and magnitude increase of the stratospheric planetary waves. For mode 2 in its positive polarity (i.e., associated with the central-Pacific El Niño–like SST), the stratospheric geopotential height anomalies show ridges and troughs to the east of those in the climatology, indicating enhanced stratospheric planetary waves with an eastward shift.

In the troposphere, both the climatological eddy and the SST-related anomalies show more latitudinal structure, and the relation between the climatology and the SST-related anomaly is not as easy to determine as in the stratosphere. These tropospheric anomalies are found to be either in phase or out of phase with the climatology, but they do not seem to introduce an east–west shift as in the stratosphere.

To better illustrate the alignment between the SST-related anomalies and the climatological waves, Fig. 7 shows a cross section at 60°S. As shown in the figure, mode 1 introduces a westward shift and mode 2 introduces an eastward shift to the climatological waves. The climatological eddies clearly show a westward tilt with height, indicating upward propagation. The SST-associated anomalies show a mixture of barotropic and baroclinic features, and the westward tilt with height is less obvious but still discernible in the stratosphere. For mode 1 (Fig. 7a), the major ridge shows a similar tilt with height as the climatological ridge. The distance between the two is about 50° throughout the stratosphere. The trough shows little tilt with height. Its distance to the climatological trough is ~100° at 100 hPa and decreases to ~50° at 1 hPa. For mode 2 (Fig. 7b), both the ridge and the trough tilt westward with height but not as much as those in the climatology. The phase difference between the mode 2 anomaly and the climatological wave is ~20° at the lower stratosphere, and increases with height, but never exceeds 90°. Such alignment between the SST-related anomalies and the climatology suggests that both modes interfere positively with the

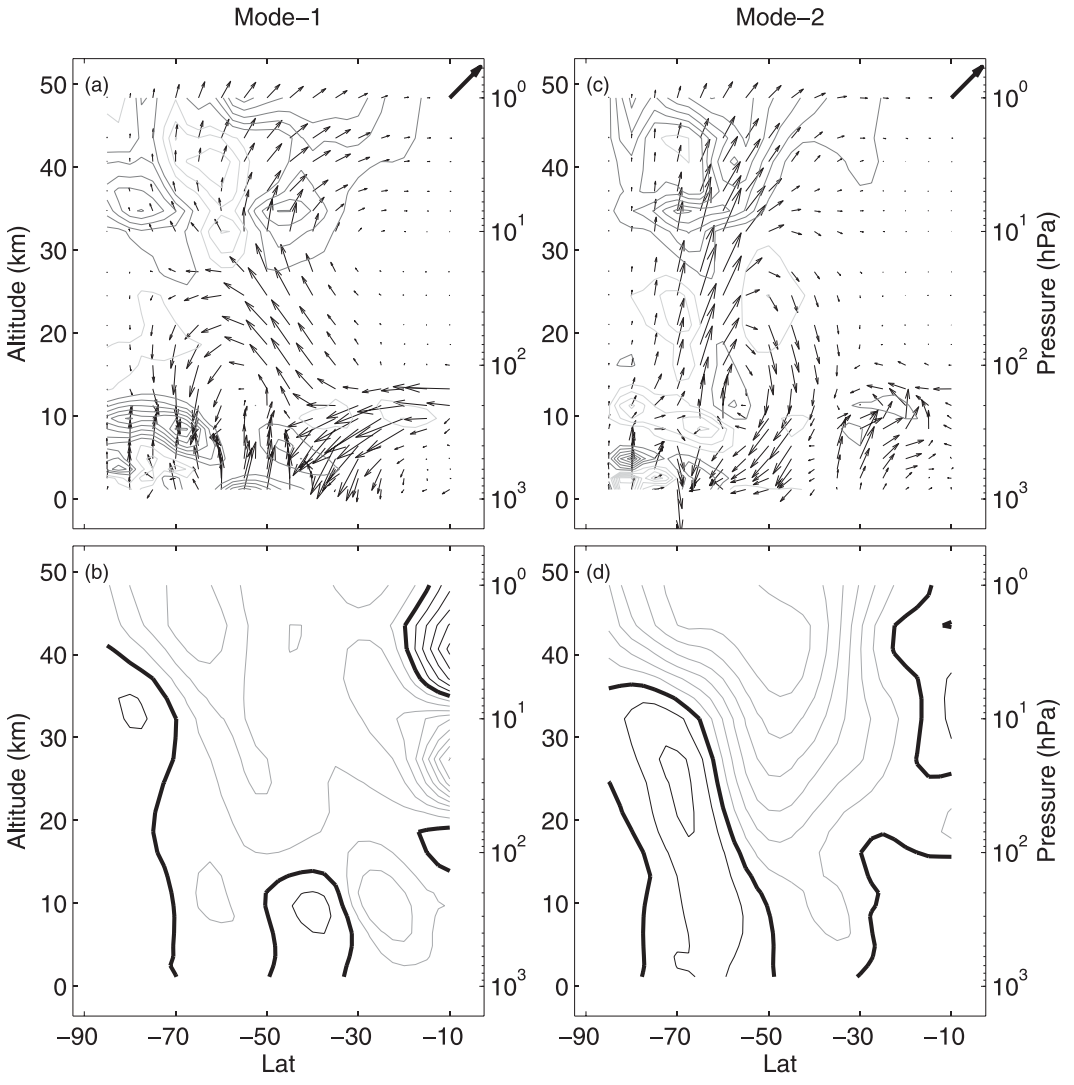

FIG. 8. (a) Regression of EP flux (vectors) and its divergence (contours) from planetary waves upon the SST time series of mode 1. EP flux vectors are scaled by $\exp(z/2H)$ to make them visible through the stratosphere as in Randel (1988), where z is the altitude and $H = 7$ km is the scale height. A reference vector is given in the top-right corner for (1, 0.005) kg m^{-1} s^{-2}. Contour interval is 0.15 m s^{-1} day^{-1}. Positive (EP flux divergence) contours are in light gray, and negative (EP flux convergence) contours are in dark gray. Zero contours are omitted. (b) Regression of zonal-mean zonal wind upon the SST time series of mode 1. Contour interval is 0.5 m s^{-1}. Easterly anomalies are plotted in thin gray lines, westerly anomalies are plotted in thin black lines, and zero contours are plotted in thick black lines. (c),(d) As in (a) and (b), but for mode 2.

climatology and so enhance the zonal asymmetry in the stratosphere.

The propagation of the anomalous wave activity associated with the two modes is diagnosed with EP flux (e.g., Andrews et al. 1987). Figures 8a,b show the regression of EP flux and its divergence from planetary waves (zonal wavenumber 1 and 2 components) upon the corresponding SST time series. More upward propagation of planetary waves into the stratosphere is associated with the positive polarity for both modes. For mode 1, the anomalous wave activity entering the stratosphere can be traced back to the midlatitude surface and to the tropical upper troposphere. But the anomalous stratospheric wave activity is traced back to the midlatitude/high-latitude upper troposphere for mode 2. Upward propagation of wave activity in the troposphere is found near 45°S for mode 1 and near 65°S for mode 2, corresponding to the places where the geopotential anomalies are found to be in phase with the climatology in the troposphere (Figs. 1d,e, k, l). These anomalous

waves spread into a broader latitudinal band, turning equatorward in the middle/upper stratosphere and breaking there over a broad region as indicated by the EP flux convergence in Figs. 8a,b. Anomalous easterlies are consistently seen there, as shown in Figs. 8c,d. The resulting wave drag can extend to 20°S in the upper stratosphere, which can provide driving for upwelling mass flux in the tropics.

4. Discussion

a. Plausible mechanisms

The mechanism of how the tropical SST can influence the stratospheric circulation is not fully understood. The tropospheric response to the tropical SST can be understood as a Rossby wave train propagating from the tropics into the extratropics (e.g., Karoly 1989; Ding et al. 2011). Some of these tropospheric anomalies can then propagate into the stratosphere and modify the stratospheric circulation, if the background state is suitable. Garfinkel and Hartmann (2008) showed that El Niño SST anomalies can enhance the NH stratospheric wave 1 by inducing a Pacific/North America (PNA) teleconnection pattern in the North Pacific. Hurwitz et al. (2011) also argued that the different SH stratospheric responses to two types of El Niño events result from the difference in the excited Rossby wave train. For the two modes identified in our work, wave train–like features can be seen emanating from the Pacific sector near the subtropical jet extending southward and eastward (Figs. 1d,e,k,l). These patterns are similar to the Rossby wave trains associated with ENSO and the central-Pacific ENSO shown by earlier studies (Ding et al. 2011; Hurwitz et al. 2011). The wave train–like features can be more clearly identified in model simulations (Figs. 4d,e,k,l).

Other studies (Robinson 2002; Seager et al. 2003; L'Heureux and Thompson 2006; Harnik et al. 2010) have interpreted the extratropical response to tropical SST as the modification of jets and eddy momentum flux. They argue that as the tropical SST warms, the stronger meridional temperature gradient will enhance the subtropical jet and shift it equatorward, and vice versa for a colder tropical SST. This change of subtropical jet will modulate the propagation and dissipation of eddies over the extratropics, especially the transient eddy momentum flux, in the upper troposphere. A stronger and more equatorward subtropical jet would lead to more equatorward momentum flux on the poleward side of the subtropical jet. As discussed in Seager et al. (2003) and L'Heureux and Thompson (2006), the anomalous transient eddy momentum flux can further induce circulation anomalies in the midlatitudes/high latitudes.

This mechanism has been used to explain the zonally symmetric response to the tropical SST. Here we showed that this also can be applied to a zonally asymmetric situation. Figure 9 shows the regression of 300-hPa zonal wind and high-frequency eddy momentum flux against the SST time series of the two modes together with the SST anomaly patterns. The high-frequency eddy is calculated from a fourth-order Butterworth filter with the cutoff at the period of 10 days. As shown in the figure, a weakened (strengthened) subtropical jet is found with the tropical cold (warm) SST anomalies. The strongest wind anomalies align with the strongest tropical SST anomalies. Strong eddy momentum flux anomalies are found on the poleward side of the subtropical wind anomalies and connect with wind anomalies in the midlatitudes. The eddy momentum flux anomalies are consistent with the wind anomalies, in the sense that positive (negative) wind is found where eddy momentum fluxes converge (diverge).

These wind and eddy momentum flux anomalies associated with the anomalous tropical SST are consistent with those suggested by earlier studies (Robinson 2002; Seager et al. 2003; L'Heureux and Thompson 2006; Harnik et al. 2010). However, it is interesting to note the strong zonal asymmetry in these anomalies (Figs. 9c,f), presumably due to the zonal asymmetry in the SST pattern itself. Thus, it is not surprising that the tropical SST can induce zonally asymmetric circulation anomalies in the extratropics through the modulation of jets and eddy momentum flux.

The two mechanisms described above to explain the extratropical response to the tropical forcing cannot be separated based on our diagnostics, and they do not necessarily exclude each other. A Rossby wave train must induce the corresponding wind and eddy momentum anomalies. In contrast, the Rossby wave source is often found near the subtropical jet core (e.g., Kidson 1999). The jet can serve as the waveguide for the Rossby waves (e.g., Ambrizzi and Hoskins 1997). Hence, the SST modulation of the jet strength and momentum fluxes is likely important in understanding the wave train structure connecting the tropics to the extratropics.

Several recent CCM studies (e.g., Shepherd and McLandress 2011; Garny et al. 2011) suggested that the major vertical wave propagation anomalies in response to warmer tropical SST occur in the subtropical region, and this is likely important for the propagation of the circulation anomaly from the troposphere to the stratosphere. These studies attribute wave propagation changes to the subtropical jet change induced by the tropical SST. In our analysis, we do observe the subtropical jet changes associated with the anomalous tropical SST patterns (Fig. 9). However, no strong vertical propagation

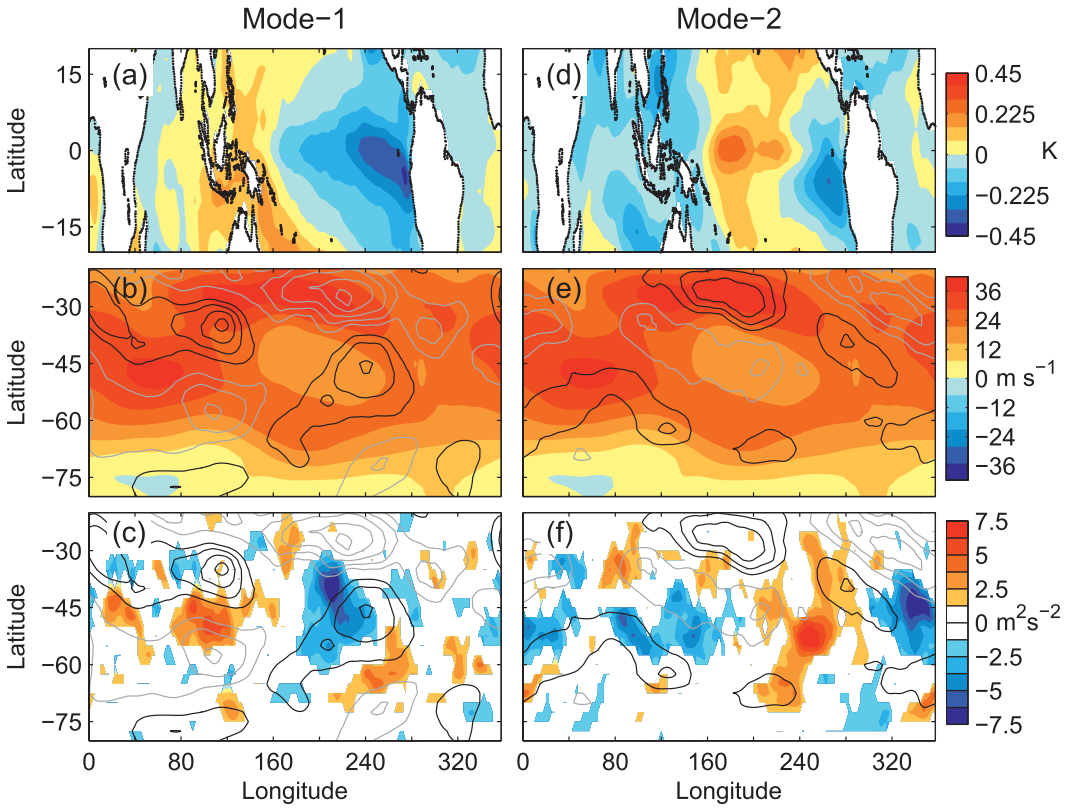

FIG. 9. (a) SST anomalies associated with mode 1. (b) Regression of zonal wind (contours) upon the SST time series and zonal wind climatology (color shading). Easterly anomalies are plotted in black lines, and westerly anomalies are plotted in gray lines. Zero contours are omitted. Contour interval is 1 m s^{-1}. (c) Regression of high-frequency eddy momentum flux (color shading) and zonal wind (contours) upon the SST time series of mode 1 at 300 hPa. Contours are the same as in (b). (d)–(f) As in (a)–(c), but for mode 2.

was seen over the subtropics (Fig. 8). Instead, we observed anomalous circulation in the extratropical troposphere associated with tropical SST, and the vertical propagation of planetary waves mainly occurred in midlatitudes/high latitudes. Ueyama and Wallace (2010) also suggested the major stratospheric wave driving should come from midlatitudes, based on satellite-borne lower-stratospheric temperature observations.

b. *Stratospheric response to ENSO and central-Pacific ENSO*

It should be noted that the diagnostic analysis in this study cannot definitely demonstrate cause and effect. However, these SST and geopotential height patterns could shed light on the underlying physical mechanisms. Because of the resemblance between our mode 1 SST pattern and the ENSO pattern, and between our mode 2 SST pattern and the central-Pacific ENSO, we compared our results with previous studies on the stratospheric response to ENSO and central-Pacific ENSO.

The impact of ENSO on the NH stratosphere during boreal winter has been discussed extensively. Both observational (e.g., Camp and Tung 2007; Garfinkel and Hartmann 2007; Free and Seidel 2009) and modeling studies (e.g., Sassi et al. 2004; Taguchi and Hartmann 2006; Manzini et al. 2006) found stronger stratospheric planetary waves associated with El Niño events during NH winter, which leads to a weaker polar vortex, stronger BDC, and warming over the pole, but cooling over the tropics. In our analysis, stronger stratospheric waves are found to be associated with La Niña–like SST in SH spring. As discussed in previous studies (Garfinkel and Hartmann 2008; Ineson and Scaife 2009; Smith et al. 2010) and here, the effect of tropical SST on the extratropical circulation depends on the position of the SST-related anomaly relative to the climatological wave. Thus, different impacts of the anomalies on the climatology can be found over different seasons and in different hemispheres.

Recently, Hurwitz et al. (2011) composited the SH eddy heat flux at 100 hPa during the September–November

(SON) season for El Niño and ENSO neutral years, and found no difference between the two cases. This disagrees with our mode 1 results. This discrepancy can be partly explained by the large monthly dependence of the extratropical stratospheric response to tropical SST. As shown in Fig. 5, almost opposite stratospheric patterns are found in October and November in response to similar ENSO-like SST anomalies. Thus, an average over SON will lead to a cancellation of the signals. Also note that our mode 1 anomaly pattern is almost in quadrature with the climatological waves at 100 hPa (Figs. 1c, 7a), but the phase difference between the anomaly and the climatology reduces at higher levels. Thus, the effect of this mode on the planetary wave amplitude may be more prominent at higher levels.

Hitchman and Rogal (2010) investigated the ENSO effect on the distribution of column ozone during the SH winter-to-spring transition. They found a westward shift of planetary waves, indicated by the column ozone pattern during La Niña events, which is consistent with our mode 1 result.

Previous studies (e.g., Camp and Tung 2007; Free and Seidel 2009) have emphasized the zonal-mean stratospheric response to the ENSO signal. Several studies (Fogt and Bromwich 2006; L'Heureux and Thompson 2006) also discussed the relation between ENSO and the southern annular mode (SAM). Here, we emphasize the effect of SST on the planetary waves but note that the waves and the zonal-mean flow are not independent from each other. Stronger waves would lead to more wave breaking in the stratosphere, which provides additional driving to the BDC and causes zonal-mean warming (higher geopotential) over the pole and cooling (lower geopotential) over the tropics. As shown in Fig. 1, the positive anomalies in the SST-related geopotential height patterns are stronger and/or extend farther zonally, indicating a zonal-mean positive geopotential height over the pole as these patterns enhance the zonal asymmetry.

The influence of the central-Pacific ENSO on the stratosphere has not been studied thoroughly because of its novelty. Studies showed that the tropospheric temperature and precipitation responses to this type of ENSO are quite different from the conventional ones (e.g., Larkin and Harrison 2005; Ashok et al. 2007; Kao and Yu 2009). Thus, a different stratospheric response should also be expected. Hurwitz et al. (2011) found stronger vertical wave propagation and a warmer pole in the SH late spring during the central-Pacific El Niño events, which agrees with our mode 2 results. But in our analysis, the central-Pacific El Niño SST structure emerged from MCA with the stratosphere and was not imposed a priori as in Hurwitz et al. (2011). The similarity of the resulting SST and atmospheric circulation anomaly patterns in the two studies suggests the robustness of these coupled patterns.

c. *Long-term trends*

Observations show warming of the lower stratosphere over Antarctica (Johanson and Fu, 2007) that is associated with a stronger BDC over the past few decades (Hu and Fu 2009; Lin et al. 2009; Fu et al. 2010). In the same period, the observed tropical SST changes favor the positive polarity of our mode 1 (e.g., Cane et al. 1997; Cravatte et al. 2009) and mode 2 (e.g., Larkin and Harrison 2005; Ashok et al. 2007; Kao and Yu 2009; Lee and McPhaden 2010). For both modes, the positive polarity is linked to a stronger stratospheric planetary wave activity and thus stronger BDC. Therefore, the tropical SST changes over the past few decades probably contribute to the observed strengthening of the BDC through both modes. How much of the currently observed tropical SST changes can be attributed to the long-term greenhouse gases increase is still a subject of debate (e.g., Tung and Zhou 2010 and references therein). Further investigation is required to understand the role of global warming in the strengthening of the BDC through the SST–stratosphere coupling.

5. Summary

The tropical SST influence on the SH stratospheric planetary wave activity is investigated in austral spring using data from the past three decades. By employing MCA on tropical SST and SH geopotential height at 50 hPa, the tropical SST and SH stratospheric planetary wave activity is found to be coupled primarily through two modes.

The first mode features an ENSO-like SST anomaly pattern, and the second mode features an SST anomaly pattern with an action center over the equatorial central Pacific. The extratropical circulation patterns associated with mode 1 are found to be robust as they can be reproduced using an independent period of data. The mode 2 patterns show less resemblance between the observations over different periods. Similar patterns for both modes are found in the multimodel mean from 14 CCM simulations, though the multimodel mean patterns show smaller amplitude than the observations. Furthermore, these patterns can vary greatly from late winter to early summer, but similar patterns are observed during months when the stratospheric basic states are similar.

These SST-related circulation anomalies are dominated by large scales and thus can modify the stratospheric planetary waves. Stronger stratospheric planetary wave activity is found to be associated with a La Niña–like SST

in mode 1, which is opposite of the situations in NH winter shown by previous studies (e.g., Camp and Tung 2007; Garfinkel and Hartmann 2007; Free and Seidel 2009; Randel et al. 2009). For mode 2, stronger wave activity is associated with warm SST anomalies over the central Pacific. These anomalous waves can be tracked back to the troposphere, and they appear to enter the stratosphere over the midlatitudes/high latitudes.

These SST-related circulation patterns are also found to affect the phase of the SH stratospheric quasi-stationary waves. For mode 1, La Niña (El Niño)-like SST anomalies induce westward (eastward) shifts to the stratospheric planetary waves. For mode 2, warm (cold) SST anomalies over the central Pacific induce eastward (westward) shifts.

The generation and propagation of the planetary wave activity is crucial to stratospheric processes, such as the BDC, ozone depletion and recovery, and stratospheric sudden warming. Thus, a better understanding of the planetary wave response to tropical SST is important, and it would be especially helpful to answer questions such as how the stratosphere will change under climate change. CCMs consistently predict a stronger BDC under climate change, but the underlying mechanisms are not well understood and vary among different models (e.g., Butchart et al. 2010; SPARC CCMVal 2010). This work may provide climate modelers with observational constrains and help resolve these questions.

Acknowledgments. We thank the anonymous reviewers for their helpful comments and suggestions. We acknowledge the modeling groups for making their simulations available for this analysis, the Chemistry–Climate Model Validation Activity (CCMVal) for the World Climate Research Programme (WCRP)'s Stratosphere–Troposphere Processes and their Role in Climate (SPARC) project for organizing and coordinating the model data analysis activity, and the British Atmospheric Data Centre (BADC) for collecting and archiving the CCMVal model output. This work is supported by NASA Grant NNX09AH73G, the National Basic Research Program of China (2010CB428604), NASA Grant NNX08AF66G, and NOAA Grant NA08OAR4310725.

REFERENCES

Ambrizzi, T., and B. J. Hoskins, 1997: Stationary Rossby-wave propagation in a baroclinic atmosphere. *Quart. J. Roy. Meteor. Soc.,* **123,** 919–928.

Andrews, D. G., J. R. Holton, and C. B. Leovy, 1987: *Middle Atmosphere Dynamics*. International Geophysical Series, Vol. 40, Academic Press, 489 pp.

Ashok, K., S. K. Behera, S. A. Rao, H. Weng, and T. Yamagata, 2007: El Niño Modoki and its possible teleconnection. *J. Geophys. Res.,* **112,** C11007, doi:10.1029/2006JC003798.

Austin, J., and N. Butchart, 1992: A three-dimensional modeling study of the influence of planetary wave dynamics on polar ozone photochemistry. *J. Geophys. Res.,* **97,** 10 165–10 186.

Bretherton, C. S., C. Smith, and J. M. Wallace, 1992: An intercomparison of methods for finding coupled patterns in climate data. *J. Climate,* **5,** 541–560.

Butchart, N., and Coauthors, 2010: Chemistry–climate model simulations of twenty-first century stratospheric climate and circulation changes. *J. Climate,* **23,** 5349–5374.

Camp, C. D., and K.-K. Tung, 2007: Stratospheric polar warming by ENSO in winter: A statistical study. *Geophys. Res. Lett.,* **34,** L04809, doi:10.1029/2006GL028521.

Cane, M. A., A. C. Clement, A. Kaplan, Y. Kushnir, D. Pozdnyakov, R. Seager, S. E. Zebiak, and R. Murtugudde, 1997: Twentieth-century sea surface temperature trends. *Science,* **275,** 957–960.

Cravatte, S., T. Delcroix, D. Zhang, M. McPhaden, and J. Leloup, 2009: Observed freshening and warming of the western Pacific warm pool. *Climate Dyn.,* **33,** 565–589, doi:10.1007/s00382-009-0526-7.

Deckert, R., and M. Dameris, 2008: Higher tropical SSTs strengthen the tropical upwelling via deep convection. *Geophys. Res. Lett.,* **35,** L10813, doi:10.1029/2008GL033719.

Ding, Q., E. J. Steig, D. S. Battisti, and M. Küettel, 2011: Winter warming in West Antarctica caused by central tropical Pacific warming. *Nat. Geosci.,* **4,** 398–403, doi:10.1038/NGEO1129.

Eichelberger, S. J., and D. L. Hartmann, 2005: Changes in the strength of the Brewer-Dobson circulation in a simple AGCM. *Geophys. Res. Lett.,* **32,** L15807, doi:10.1029/2005GL022924.

Eyring, V., and Coauthors, 2005: A strategy for process-oriented validation of coupled chemistry–climate models. *Bull. Amer. Meteor. Soc.,* **86,** 1117–1133.

Fogt, R. L., and D. H. Bromwich, 2006: Decadal variability of the ENSO teleconnection to the high-latitude South Pacific governed by coupling with the southern annular mode. *J. Climate,* **19,** 979–997.

Free, M., and D. J. Seidel, 2009: Observed El Niño–Southern Oscillation temperature signal in the stratosphere. *J. Geophys. Res.,* **114,** D23108, doi:10.1029/2009JD012420.

Fu, Q., S. Solomon, and P. Lin, 2010: On the seasonal dependence of tropical lower-stratospheric temperature trends. *Atmos. Chem. Phys.,* **10,** 2643–2653.

Fusco, A. C., and M. L. Salby, 1999: Interannual variations of total ozone and their relationship to variations of planetary wave activity. *J. Climate,* **12,** 1619–1629.

Garfinkel, C. I., and D. L. Hartmann, 2007: Effects of the El Niño–Southern Oscillation and the quasi-biennial oscillation on polar temperatures in the stratosphere. *J. Geophys. Res.,* **112,** D19112, doi:10.1029/2007JD008481.

——, and ——, 2008: Different ENSO teleconnections and their effects on the stratospheric polar vortex. *J. Geophys. Res.,* **113,** D18114, doi:10.1029/2008JD009920.

Garny, H., M. Dameris, W. J. Randel, G. E. Bodeker, and R. Deckert, 2011: Dynamically forced increase of tropical upwelling in the lower stratosphere. *J. Atmos. Sci.,* **68,** 1214–1233.

Grassi, B., G. Redaelli, and G. Visconti, 2008: Tropical SST preconditioning of the SH polar vortex during winter 2002. *J. Climate,* **21,** 5295–5303.

Harnik, N., R. Seager, N. Naik, M. Cane, and M. Ting, 2010: The role of linear wave refraction in the transient eddy-mean flow response to tropical Pacific SST anomalies. *Quart. J. Roy. Meteor. Soc.,* **136,** 2132–2146.

Hitchman, M. H., and M. J. Rogal, 2010: ENSO influences on Southern Hemisphere column ozone during the winter to spring transition. *J. Geophys. Res.,* **115,** D20104, doi:10.1029/2009JD012844.

Holton, J. R., P. H. Haynes, M. E. McIntyre, A. R. Douglass, R. B. Rood, and L. Pfister, 1995: Stratosphere-troposphere exchange. *Rev. Geophys.,* **33,** 403–439, doi:10.1029/95RG02097.

Hu, Y., and Q. Fu, 2009: Stratospheric warming in Southern Hemisphere high latitudes since 1979. *Atmos. Chem. Phys.,* **9,** 4329–4340.

Hurwitz, M. M., P. A. Newman, L. D. Oman, and A. M. Molod, 2011: Response of the Antarctic stratosphere to two types of El Niño events. *J. Atmos. Sci.,* **68,** 812–822.

Inatsu, M., and B. J. Hoskins, 2004: The zonal asymmetry of the Southern Hemisphere winter storm track. *J. Climate,* **17,** 4882–4892.

Ineson, S., and A. A. Scaife, 2009: The role of the stratosphere in the European climate response to El Niño. *Nat. Geosci.,* **2,** 32–36.

Johanson, C. M., and Q. Fu, 2007: Antarctic atmospheric temperature trend patterns from satellite observations. *Geophys. Res. Lett.,* **34,** L12703, doi:10.1029/2006GL029108.

Kalnay, E., and Coauthors, 1996: The NCEP/NCAR 40-Year Reanalysis Project. *Bull. Amer. Meteor. Soc.,* **77,** 437–471.

Kanamitsu, M., W. Ebisuzaki, J. Woolen, S.-K. Yang, J. J. Hnilo, M. Fiorino, and G. L. Potter, 2002: NCEP–DOE AMIP-II Reanalysis (R-2). *Bull. Amer. Meteor. Soc.,* **83,** 1631–1643.

Kao, H.-Y., and J.-Y. Yu, 2009: Contrasting eastern-Pacific and central-Pacific types of ENSO. *J. Climate,* **22,** 615–632.

Karoly, D. J., 1989: Southern Hemisphere circulation features associated with El Niño–Southern Oscillation events. *J. Climate,* **2,** 1239–1252.

——, and B. J. Hoskins, 1982: Three dimensional propagation of planetary waves. *J. Meteor. Soc. Japan,* **60,** 109–123.

Kasahara, A., and P. L. da Silva Dias, 1986: Response of planetary waves to stationary tropical heating in a global atmosphere with meridional and vertical shear. *J. Atmos. Sci.,* **43,** 1893–1912.

Kawamura, R., 1994: A rotated EOF analysis of global sea surface temperature variability with interannual and interdecadal scales. *J. Phys. Oceanogr.,* **24,** 707–715.

Kidson, J. W., 1999: Principal modes of Southern Hemisphere low-frequency variability obtained from NCEP–NCAR reanalyses. *J. Climate,* **12,** 2808–2830.

Kug, J.-S., F.-F. Jin, and S.-I. An, 2009: Two types of El Niño events: Cold tongue El Niño and warm pool El Niño. *J. Climate,* **22,** 1499–1515.

Larkin, N. K., and D. E. Harrison, 2005: Global seasonal temperature and precipitation anomalies during El Niño autumn and winter. *Geophys. Res. Lett.,* **32,** L16705, doi:10.1029/2005GL022860.

Lee, T., and M. J. McPhaden, 2010: Increasing intensity of El Niño in the central-equatorial Pacific. *Geophys. Res. Lett.,* **37,** L14603, doi:10.1029/2010GL044007.

L'Heureux, M. L., and D. W. J. Thompson, 2006: Observed relationships between the El Niño–Southern Oscillation and the extratropical zonal-mean circulation. *J. Climate,* **19,** 276–287.

Li, F., R. S. Stolarski, and P. A. Newman, 2009: Stratospheric ozone in the post-CFC era. *Atmos. Chem. Phys.,* **9,** 2207–2213.

Li, S., J. Perlwitz, M. P. Hoerling, and X. Chen, 2010: Opposite annular responses of the Northern and Southern Hemispheres to Indian Ocean warming. *J. Climate,* **23,** 3720–3738.

Lin, P., Q. Fu, S. Solomon, and J. M. Wallace, 2009: Temperature trend patterns in Southern Hemisphere high latitudes: Novel indicators of stratospheric change. *J. Climate,* **22,** 6325–6341.

Manzini, E., M. A. Giorgetta, M. Esch, L. Kornblueh, and E. Roeckner, 2006: The influence of sea surface temperatures on the northern winter stratosphere: Ensemble simulations with the MAECHAM5 model. *J. Climate,* **19,** 3863–3881.

Mechoso, C. R., D. L. Hartmann, and J. D. Farrara, 1985: Climatology and interannual variability of wave, mean-flow interaction in the Southern Hemisphere. *J. Atmos. Sci.,* **42,** 2189–2206.

Olsen, M. A., M. R. Schoeberl, and J. E. Nielsen, 2007: Response of stratospheric circulation and stratosphere-troposphere exchange to changing sea surface temperatures. *J. Geophys. Res.,* **112,** D16104, doi:10.1029/2006JD008012.

Oman, L. D., D. W. Waugh, S. Pawson, R. S. Stolarski, and P. A. Newman, 2009: On the influence of anthropogenic forcings on changes in the stratospheric mean age. *J. Geophys. Res.,* **114,** D03105, doi:10.1029/2008JD010378.

——, and Coauthors, 2010: Multimodel assessment of the factors driving stratospheric ozone evolution over the 21st century. *J. Geophys. Res.,* **115,** D24306, doi:10.1029/2010JD014362.

Onogi, K., and Coauthors, 2007: The JRA-25 Reanalysis. *J. Meteor. Soc. Japan,* **85,** 369–432.

Polvani, L. M., and R. A. Plumb, 1992: Rossby wave breaking, microbreaking, filamentation, and secondary vortex formation: The dynamics of a perturbed vortex. *J. Atmos. Sci.,* **49,** 462–476.

Quintanar, A. I., and C. R. Mechoso, 1995: Quasi-stationary waves in the Southern Hemisphere. Part II: Generation mechanisms. *J. Climate,* **8,** 2673–2690.

Randel, W. J., 1988: The seasonal evolution of planetary waves in the Southern Hemisphere stratosphere and troposphere. *Quart. J. Roy. Meteor. Soc.,* **114,** 1385–1409.

——, R. R. Garcia, N. Calvo, and D. Marsh, 2009: ENSO influence on zonal mean temperature and ozone in the tropical lower stratosphere. *Geophys. Res. Lett.,* **36,** L15822, doi:10.1029/2009GL039343.

Rayner, N. A., D. E. Parker, E. B. Horton, C. K. Folland, L. V. Alexander, D. P. Rowell, E. C. Kent, and A. Kaplan, 2003: Global analyses of sea surface temperature, sea ice, and night marine air temperature since the late nineteen century. *J. Geophys. Res.,* **108,** 4407, doi:10.1029/2002JD002670.

Rienecker, M. M., and Coauthors, 2011: MERRA: NASA's Modern-Era Retrospective Analysis for Research and Applications. *J. Climate,* **24,** 3624–3648.

Robinson, W. A., 2002: On the midlatitude thermal response to tropical warmth. *Geophys. Res. Lett.,* **29,** 1190, doi:10.1029/2001GL014158.

Rosenlof, K. H., and J. R. Holton, 1993: Estimates of the stratospheric residual circulation using the downward control principle. *J. Geophys. Res.,* **98,** 10 465–10 479.

Sassi, F., D. Kinneson, B. A. Boville, R. R. Garcia, and R. Roble, 2004: Effect of El Niño–Southern Oscillation on the dynamical, thermal, and chemical structure of the middle atmosphere. *J. Geophys. Res.,* **109,** D17108, doi:10.1029/2003JD004434.

Seager, R., N. Harnik, and Y. Kushnir, 2003: Mechanisms of hemispherically symmetric climate variability. *J. Climate,* **16,** 2960–2978.

Shepherd, T. G., and C. McLandress, 2011: A robust mechanism for strengthening of the Brewer–Dobson circulation in response to climate change: Critical-layer control of subtropical wave breaking. *J. Atmos. Sci.,* **68,** 784–797.

Smith, K. L., C. G. Fletcher, and P. J. Kushner, 2010: The role of linear interference in the annular mode response to extratropical surface forcing. *J. Climate,* **23,** 6036–6050.

Smith, T. M., R. W. Reynolds, T. C. Peterson, and J. Lawrimore, 2008: Improvements to NOAA's historical merged land–ocean surface temperature analysis (1880–2006). *J. Climate,* **21,** 2283–2296.

Solomon, S., 1999: Stratospheric ozone depletion: A review of concepts and history. *Rev. Geophys.,* **37,** 275–316, doi:10.1029/1999RG900008.

SPARC CCMVal, 2010: SPARC report on the evaluation of Chemistry-Climate Models. V. Eyring, T. G. Shepherd, D. W. Waugh, Eds., SPARC Rep. 5, WCRP-132, WMO/TD-1526, 499 pp. [Available online at http://www.sparc-climate.org/publications/sparc-reports/sparc-report-no5/.]

Taguchi, M., and D. L. Hartmann, 2006: Increased occurrence of stratospheric sudden warmings during El Niño as simulated by WACCM. *J. Climate,* **19,** 324–332.

Thompson, D. W. J., and S. Solomon, 2002: Interpretation of recent Southern Hemisphere climate change. *Science,* **296,** 895–899.

Trenberth, K. E., 1997: The definition of El Niño. *Bull. Amer. Meteor. Soc.,* **78,** 2771–2777.

Tung, K.-K., and J. Zhou, 2010: The Pacific's response to surface heating in 130 yr of SST: La Niña–like or El Niño–like? *J. Atmos. Sci.,* **67,** 2647–2657.

Ueyama, R., and J. M. Wallace, 2010: To what extent does high-latitude wave forcing drive tropical upwelling in the Brewer–Dobson circulation? *J. Atmos. Sci.,* **67,** 1232–1246.

Uppala, S. M., and Coauthors, 2005: The ERA-40 Re-Analysis. *Quart. J. Roy. Meteor. Soc.,* **131,** 2961–3012.

Wallace, J. M., C. Smith, and C. S. Bretherton, 1992: Singular value decomposition of wintertime sea surface temperature and 500-mb height anomalies. *J. Climate,* **5,** 561–576.